

## Ultrasonic Synthesis of Polysodium-4-styrene Sulfonate coated Functionalized MWCNTs for Electrochemical Detection of Anti-Oxidant Drug in Red Wine

Ragu Sasikumar<sup>1</sup>, Tse-Wei Chen<sup>1,2</sup>, Shen-Ming Chen<sup>1,2,\*</sup>, Yu Chi Chen<sup>1</sup>, Syang-Peng Rwei<sup>2,3</sup>

<sup>1</sup> Department of Chemical Engineering and Biotechnology, National Taipei University of Technology, No. 1, Section 3, Chung-Hsiao East Road, Taipei 106, Taiwan, ROC.

<sup>2</sup> Research and Development Center for Smart Textile Technology, National Taipei University of Technology, Taipei 106, Taiwan, ROC

<sup>3</sup> Institute of Organic and Polymeric Materials, National Taipei University of Technology, Taipei 106, Taiwan, ROC

\*E-mail: [smchen78@ms15.hinet.net](mailto:smchen78@ms15.hinet.net).

Received: 11 June 2018/ Accepted: 12 August 2018 / Published: 1 September 2018

---

A greatly selective, and sensitive 3,4-Dihydroxy-trans-cinnamate sensor based on a poly (sodium 4-styrenesulfonate) (PSSS) coated with functionalized multiwalled carbon nanotubes (PSSS@f-MWCNTs) composite modified electrode was improved. The fabricated PSSS@f-MWCNTs/GCE displayed an excellent voltammetric response for caffeic acid to compared control electrodes. Under optimum conditions, the modified electrode showed a wide linear range at caffeic acid concentrations of 0.4–173.9  $\mu\text{M}$ . The limit of detection is 35 nM and sensitivity is 17.44  $\mu\text{A } \mu\text{M}^{-1}\text{cm}^{-2}$ . The improved sensor method was showed good anti-interference, reproducibility, good repeatability, and excellent storage stability.

---

**Keywords:** Poly (sodium 4-styrenesulfonate), 3,4-Dihydroxy-trans-cinnamate, TGA, Co-polymer, Ionic polymer.

### 1. INTRODUCTION

The current magnification of avail in carbon based materials has opened incipient ways for engendering arrays of unorthodox functional nanomaterials. Graphene is a two-dimensional (2D NM) nanomaterial, and it is composed of several planar sheets of  $\text{sp}^2$ -bonded carbon atoms arranged in six-membered ringing, has magnetized tremendous attention from scientific communities due to its unique properties such as thermal, chemical, physical, mechanical, and electrical properties [1-6]. Graphene

and graphene based materials have been emerging as a promising candidate for engendering novel hybrid nanomaterials with their excellent properties for a wide potpourri of potential drop applications in expeditor support, electronic components, chemical sensing element, and Li ion batteries [7-12]. Kindred to the early days of carbon nanotube research, recently, a novel class of carbon-coated functional nanomaterials have been developed to optimize the electrical, optical, biological, and catalyst properties via the coalescence of graphene with metal nanoparticles [13-15]. As a novel carbon material, graphene is highly expected as a frugal substitute for MWCNTs to provide a cost-efficacious platform for developing hybrid materials containing graphene, and metal nanoparticles because it possesses sizably voluminous interfacial surface area far much better than MWCNTs [16-19]. Hence, it is believed that the dispersion of metal nanoparticles on graphene sheets opens incipient ways for researchers in designing hybrid materials for sundry potential applications [20, 21]. Poly (sodium 4-styrenesulfonate) (PSSS) is a polyelectrolyte with excellent biocompatibility, mechanical, electrical, and selectivity properties [22, 23].

Polyphenolic compounds are known as poly hydroxyphenols in plant life and are present in plant-derived foods including grapes, apples, citrus fruit, berries, and cocoa; vegetables such as soybeans, olives, tomatoes, onions, and broccoli; cereals, and grains; black and green teas, propolis, and white and red wines [24]. Gallic, and caffeic acids are the familiar medicinal, pharmacological, and biochemical properties of phenolics have been widely studied. Among these, caffeic acid (CA) has been found to be customarily subsisting in higher plants in different forms such as esters, glycosides, and the free form [25]. CA is one of the antioxidant chemical [24]. For example, the caffeic acid phenethyl esters that occur in honeybee hive products have both immunomodulatory, and anti-carcinogenic properties. Derivatives of caffeic acid are copious in wine [26]. The phenolic derivative of caffeic acid are the key suppliers to color stability and shield beside oxidation in the wine [26]. To increment the electrochemical performance, we prepared the PSSS polymer doped *f*-MWCNTs, which may have an excellent electro catalytic activity, and electron conductivity owing to the coalescence of PSSS, and *f*-MWCNTs. In this present study, PSSS decorated on functionalized multiwalled carbon nanotubes (PSSS@*f*-MWCNTs) composite prepared by facile ultrasonic method. The as-prepared composite was characterized by various analytical techniques.

## 2. EXPERIMENTAL PART

### 2.1. Materials and Instrumentation

Pristine MWCNTs (>95%, outer diameter 20-30 nm), poly (sodium 4-styrene sulfonate) sodium salt (PSSS) (molecular weight ~1,000,000), sulfuric acid (95-98%), nitric acid (70%), ethanol ( $\geq 99.8\%$ ), caffeic acid ( $\geq 98\%$ ), were obtained from Sigma-Aldrich. All the solvents, chemicals, and reagents used were of analytical grade. The crystalline structure of the PSSS@*f*-MWCNTs composite was characterized by powder X-ray diffraction (PXRD) by XPERT-PRO (PANalytical B.V., The Netherlands) diffractometer (Cu  $K\alpha$  radiation,  $\lambda=1.54 \text{ \AA}$ ). Thermogravimetric analysis (TGA) measurements were performed using a Netzsch TG-209 series apparatus at a heating rate of  $10 \text{ }^\circ\text{C min}^{-1}$  under a constant flow of nitrogen. The morphology of the nanocomposite was studied by scanning

electron microscopy (SEM) at room temperature (25 °C) using SEM (Hitachi S-3000 H). The chemical compositions and orientations of the grains were studied by Transmission electron microscope (TEM) using a JEOL 2000 operating at 200 kV. An EIM6ex Zahner (Kronach, Germany) was used for electrochemical was used for electrochemical impedance spectroscopy (EIS) studies. The electrochemical response of PSSS@*f*-MWCNTs composite studied by cyclic voltammetry (CV), and differential pulse voltammetry (DPV) using CHI 1205a, and CHI 900 electrochemical analyzer (CH instruments).

## 2.2. Preparation of PSSS@*f*-MWCNTs

The *f*-MWCNTs were prepared by oxidation with HNO<sub>3</sub>/H<sub>2</sub>SO<sub>4</sub>. Pre-determined amounts of pristine MWCNTs, and 250 mL of 3:1 ratio of HNO<sub>3</sub>/H<sub>2</sub>SO<sub>4</sub> were dispersed for 1 h in an ultrasonic bath [27]. The dispersed solutions were kept in the reaction flask at 120 °C for 72 h and it affixed with reflux condenser, and magnetic stirrer. The *f*-MWCNTs were cooled to the room temperature, and extra solvents were removed by vacuum filtered then washed with water. 0.05 g of *f*-MWCNT, and 0.05 g of PSSS was ultrasonicate in 1 mL of water for 1 h, and used for further studies. The general synthesis way for PSSS@*f*-MWCNTs composite as showed in Scheme 1.



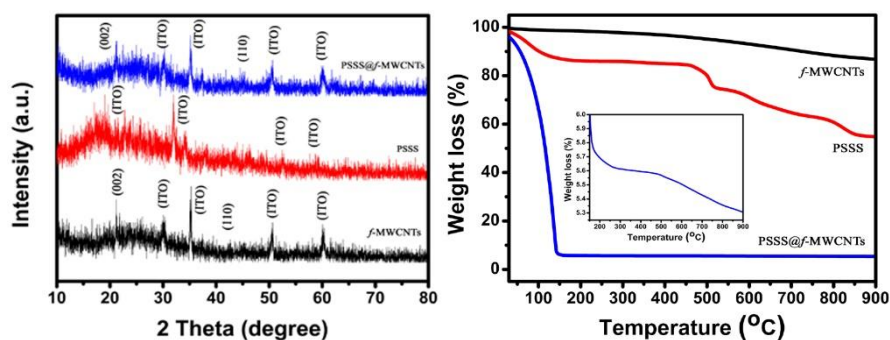
**Scheme 1.** Preparation of PSSS@*f*-MWCNTs composite.

## 3. RESULTS AND DISCUSSION

### 3.1. Characterization of PSSS@*f*-MWCNTs nanocomposite

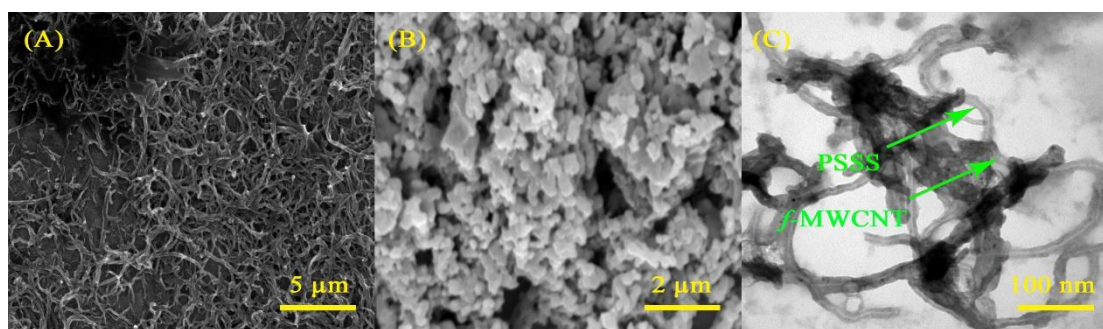
The XRD peaks of *f*-MWCNTs, PSSS, and PSSS@*f*-MWCNTs are shown in Figure 1A. For *f*-MWCNTs the diffraction peaks are appeared at  $2\theta = 21^\circ$  and  $42.6^\circ$  (due to the corresponding planes are ((002), (100)), and broad peak observed between  $15\text{-}25^\circ$  due to the amorphous nature of carbon material. For PSSS polymer, the visible broad peak observed between  $15\text{-}25^\circ$  owing to the amorphous nature of PSSS as shown in Figure 1A [28]. Finally, PSSS@*f*-MWCNTs composite, PXRD peaks are observed  $2\theta = 21.1^\circ$ , and  $45.2^\circ$  are due to the (002), and (110) planes. The carbon material amorphous broad peak also appeared  $2\theta$  range between  $15\text{-}25^\circ$  [29]. Thermal stability of *f*-MWCNTs, PSSS, and PSSS@*f*-MWCNTs composite was additional considered by TGA as shown in Figure 1B. For *f*-MWCNTs the gradual weight loss observed from 25 to 900 °C (due to removal of H<sub>2</sub>O, H<sub>2</sub>, CH<sub>4</sub> etc.). PSSS polymer the weight loss detected in three stages. Solvents, and absorbed water are eliminating at

130 °C, and other molecules like H<sub>2</sub>, CH<sub>4</sub>, SO<sub>2</sub>, and SO<sub>3</sub> are removed from 130 to 900 °C. The nanocomposite was heated from ambient temperature at 900 °C. The weight residue studied from 25 to 900 °C.



**Figure 1.** (A) XRD, and (B) TGA curve of PSSS@f-MWCNTs.

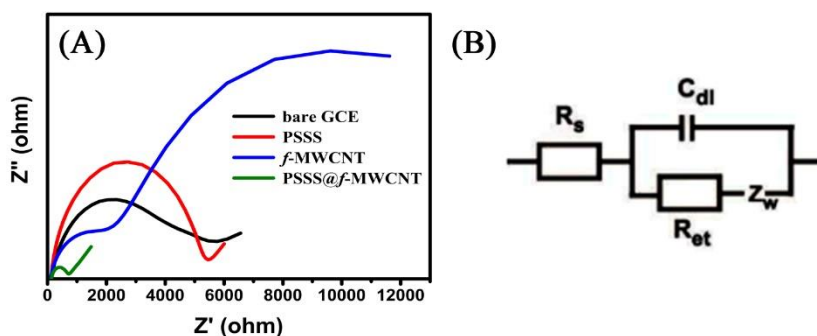
Figure 2 (A-C) displayed SEM, and TEM images of f-MWCNT, PSSS, and PSSS@f-MWCNTs composite. Figure 2A, showed that these carbon nanotubes have uniform structure. Figure 2B displayed PSSS polymer, and it looks like agglomeration. Figure 2C showed TEM images of as-prepared nanocomposite it shows like nano tubes coated with PSSS polymer is confirmed. This composite slightly amorphous nature, and is compared with XRD analysis.



**Figure 2.** (A, B) SEM images of f-MWCNT, PSSS, and (C) TEM image of PSSS@f-MWCNTs nanocomposite.

### 3.2. Electrochemical impedance spectroscopy of nanocomposite

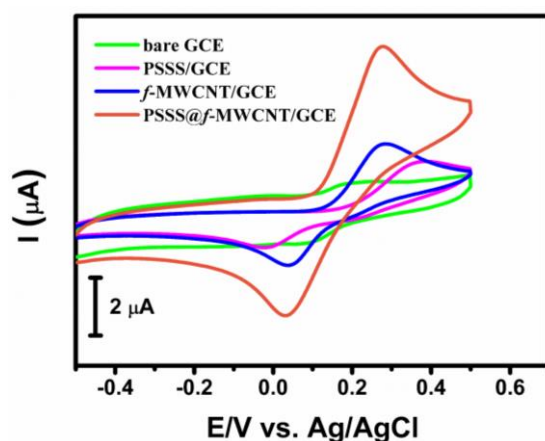
To study the conductivity, and electroactive surface area at the electrolyte/electrode interfaces, the EIS study is achieved. The diameter of the semicircle is a direct illustration of the charge transfer resistance ( $R_{ct}$ ). Figure 3A shows the Nyquist plots of bare electrode, f-MWCNT/GCE, PSSS/GCE, and PSSS@f-MWCNT/GCE, studied in 1 mM of [Fe(CN)<sub>6</sub>]<sup>3-/4-</sup>, and 0.1 M of KCl were used as the supporting electrolyte solution. Figure 3A and 3B display that the PSSS, and bare electrode has higher  $R_{ct}$  when compared with the other modified electrodes. Hence, the PSSS@f-MWCNTs modified electrode exhibits the lowest  $R_{ct}$  value compared to other modified electrode, which suggests the PSSS@f-MWCNTs could be used as an optimized electrode for electrochemical sensor application.



**Figure 3.** (A) EIS plots of 1.0 mM  $[\text{Fe}(\text{CN})_6]^{3-/4-}$  in 0.1 M KCl noted at bare GCE,  $f$ -MWCNT/GCE, PSSS/GCE, and PSSS@ $f$ -MWCNT/GCE, and (B) Randles equivalent circuit model.

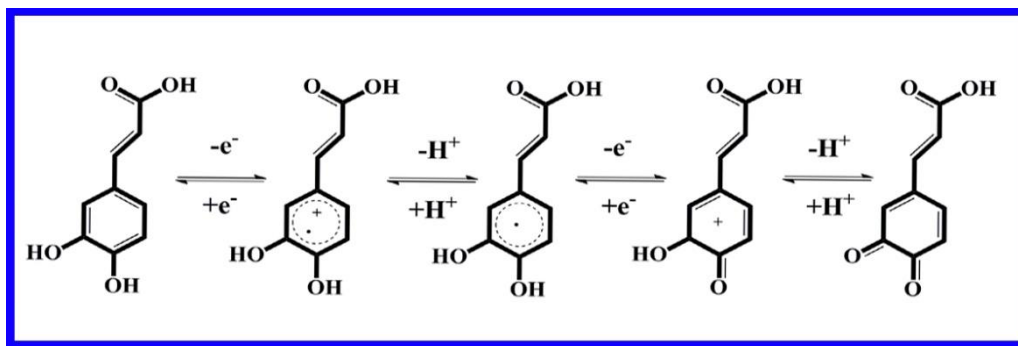
### 3.3. Electrocatalytic activity of CA at different modified electrodes

Figure 4 shows the CVs at bare GCE, PSSS/GCE,  $f$ -MWCNTs/GCE, and PSSS@ $f$ -MWCNTs/GCE with 200  $\mu\text{M}$  of CA in PB (pH 7.0, Scan rate of 50  $\text{mV s}^{-1}$ ). Moreover, CA at bare GCE displays small difference in the CV curve with a low current peak. Furthermore, a considerable signals observed at 386 mV and 286 mV for the PSSS, and  $f$ -MWCNTs/GCEs respectively. The well-marked anodic current was detected at 0.278 V for the PSSS@ $f$ -MWCNTs/GCE as shown in Figure 4. Finally, the results, shows that the electrocatalytic behavior of CA has a reversible two protons, and two electrons transfer process. The electrochemical oxidation of CA is shown in Scheme 2 [30].



**Figure 4.** CV response of bare GCE, PSSS/GCE,  $f$ -MWCNTs/GCE, and PSSS@ $f$ -MWCNT/GCE with 200  $\mu\text{M}$  CA in 0.05 M PB (pH 7).

However, PSSS@ $f$ -MWCNTs modified electrode is showed maximum electrocatalytic ability compared to bare GCE, PSSS/GCE,  $f$ -MWCNTs/GCE. Thus, PSSS@ $f$ -MWCNTs/GCE has a greater electrocatalytic performance to the oxidation of CA due the interaction between PSSS and  $f$ -MWCNTs in the nanocomposite. The huge anodic peaks happen at peak potentials of 0.27 V due to  $2e^-$ , and  $2\text{H}^+$  oxidation of the CA (Scheme 2).



**Scheme 2.** Electrocatalytic Oxidation of CA.

### 3.4. Effect of scan rate

The effect of scan rate was studied using PSSS@*f*-MWCNT/GCE in PB (pH 7). The oxidation peak current increasing the anodic peaks from 20 to 200  $\text{mV s}^{-1}$  is observed in CV curves Figure 5A. When the oxidation peaks current ( $I_{pa}$ ) increases the scan rate also increases linearly. Moreover, the linear plot of scan rate was studied in Figure 5B. The oxidation process of CA appeared at the PSSS@*f*-MWCNT modified electrode is diffusion controlled process Figure 5B. Furthermore, the obtained linear regression equations are  $E_{pa} (\text{V}) = 0.038x + 1.172$ ,  $R^2 = 0.992$ , and  $E_{pc} (\text{V}) = 0.0315x - 0.570$ ,  $R^2 = 0.990$ . This shows that the influence of adsorption frolicked an important role in the electrode reaction, owing to the fact that the affinity, and the surface accumulation process of CA was slow on the PSSS modified electrode. This suggests that the overall oxidation, and reduction of CA at the PSSS@*f*-MWCNT modified electrode is controlled by an adsorption phenomenon [26].

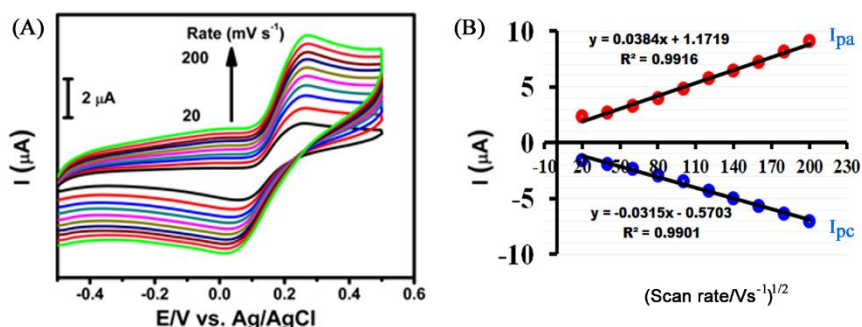


**Figure 5.** (A) CVs obtained at PSSS@*f*-MWCNT/GCE in PB (pH 7) containing 200  $\mu\text{M}$  of CA at 20 to 200  $\text{mV s}^{-1}$ , and (B) The plot between oxidation peak current vs square root of scan rate.

### 3.5. Determination of CA

Determination of CA was studied at PSSS@*f*-MWCNT modified electrode using DPV as shown in the Figure 6A. The DPV response of the PSSS@*f*-MWCNT with the additions of different concentration of CA containing PB (pH 7). The sensitivity was analyzed by DPV using slope of the calibration plot as shown in the Figure 6B. The sensitivity is  $14.91 (\pm 0.002) \mu\text{A } \mu\text{M}^{-1} \text{ cm}^{-2}$ , and linear

range is 0.4-173.9  $\mu\text{M}$ . The limit of detection (LOD) was calculated as 35 nM based on a signal-to-noise ratio equal to (n) 3. The observed LOD is better than those of previously reported modified electrodes in Table 1. A linear relationship between CA concentration vs peak current ( $I_{\text{pa}}$ ) was obtained using 0.4-173.9  $\mu\text{M}$  CA, linear regression equation, and correlation co-efficient are  $I_{\text{pa}} = 1.258x + 1.7817$ , and  $R^2 = 0.996$  respectively.

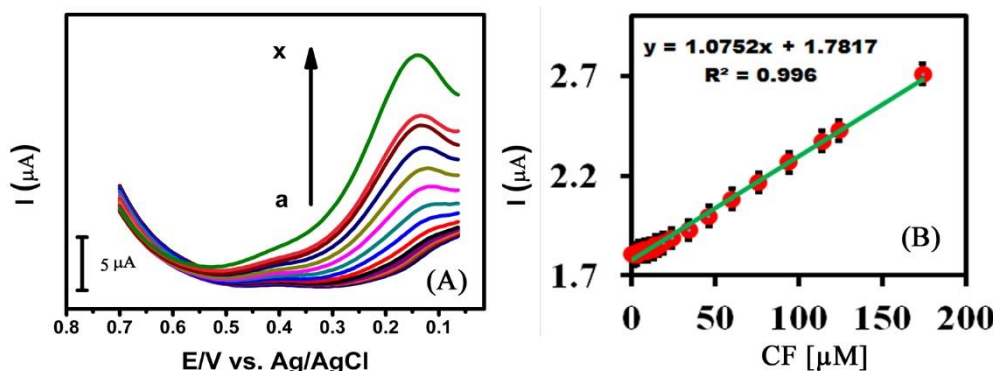


**Figure 6.** (A) DPVs of increasing CA concentration (a–x = 0.4–173.9  $\mu\text{M}$ ), and (B) Peak currents vs [CA].

**Table 1.** Comparison of analytical performance of CA sensor with previously reports.

Electrode	Limit of detection ( $\mu\text{M}$ )	Linear range ( $\mu\text{M}$ )	Ref
Au/graphene	50	0.5-50	28
Au-PEDOT/RGO	4	0.01-46	29
Au/CS	25	0.05-2000	30
MWNTs-[BuPy]PF6-CS	5.7	0.025-7	31
CRGO	2	0.1-800	27
G-quadruplex/hemin	200	2-350	32
ERGO/Nafion	9.1	0.1-1.5	17
ZrO <sub>2</sub> /Co <sub>3</sub> O <sub>4</sub> /RGO	0.62	0.00248-0.525	33
<b>PSSS@f-MWCNT</b>	<b>0.035</b>	<b>0.4-173.9</b>	<b>This work</b>

RGO=reduced graphene oxide, CS=chitosan, MWNTs-[BuPy]PF6=Multiwalled carbon Nanotubes-N-Butylpyridinium hexafluorophosphate ionic liquid, CRGO=Chemically reduced graphene oxide, ERGO=Electrochemically reduced graphene oxide.

### 3.6. Interference study

The anti-interference study of the modified sensor was studied by DPV in the presence of 50  $\mu\text{M}$  CA and 50-fold excess concentrations of hydroquinone (HQ), dopamine (DA), epinephrine (EP), uric acid (UA), catechol (CT), ascorbic acid (AA), 100-fold excess concentrations of calcium ( $\text{Ca}^{2+}$ ), mercury ( $\text{Hg}^{2+}$ ), potassium ( $\text{K}^+$ ), sodium ( $\text{Na}^{2+}$ ), lead ( $\text{Pb}^{2+}$ ), zinc ( $\text{Zn}^{2+}$ ), and chromium ( $\text{Cr}^{2+}$ ), and the found results are shown in Figure 7. Figure 7 clearly representations that the  $\text{Ca}^{2+}$ ,  $\text{Hg}^{2+}$ ,  $\text{K}^+$ ,  $\text{Na}^{2+}$ ,

$Pb^{2+}$ ,  $Zn^{2+}$ , and  $Cr^{2+}$  didn't show any obvious response at PSSS@*f*-MWCNT/GCE; whereas, HQ, DA, EP, UA, CT, and AA displayed a minor reply at the potential of 0.278 V. Though, HQ, EP, UA, CT, and AA didn't interrupt the oxidation peak potential of CA, while, a slight change in the oxidation peak potential was noticed in presence of DA. The results undoubtedly showed that the interference effect of HQ, EP, UA, CT, and AA is irrelevant for the detection of CA at PSSS@*f*-MWCNT/GCE. The result designates that the good selectivity of the developed sensor.

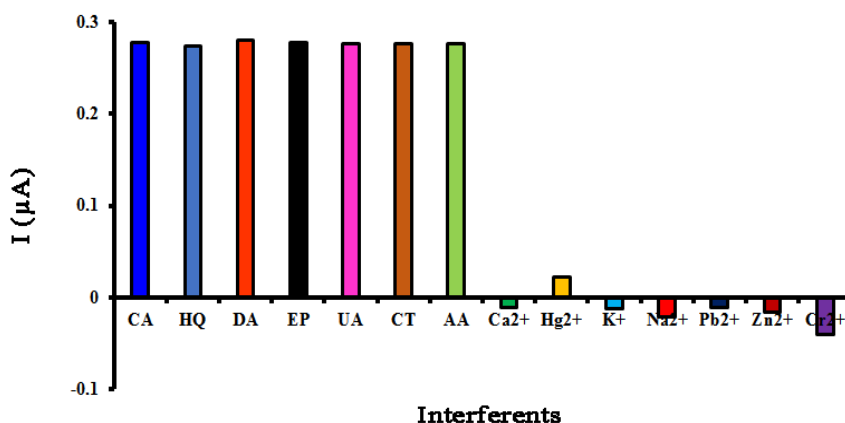


**Figure 7.** Change in DPV current response (%) of PSSS@*f*-MWCNTs/GCE for CA in the presence of additions of different metal ions, and biological compounds.

### 3.7. Studies of accumulation time, reproducibility, and storage stability

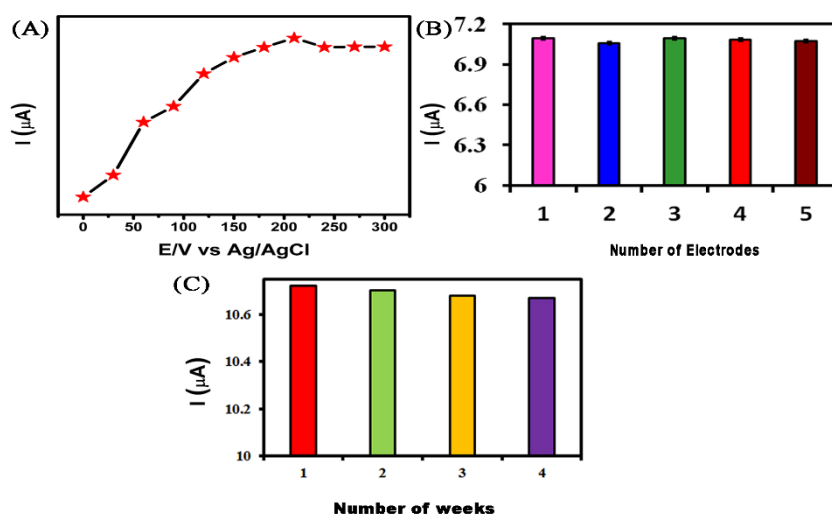


**Figure 8.** CVs found at (A) accumulation time observed at PSSS@*f*-MWCNTs/GCE in PBS (pH 7) containing 200 μM CA (B) reproducibility of PSSS@*f*-MWCNTs/GCE in PB (pH 7) containing 200 μM CA at five different electrodes, and (C) Storage stability of PSSS@*f*-MWCNTs/GCE.

To observe the effects of an accumulation time in the oxidation of CA, the CV curve were noted for PSSS@*f*-MWCNT/GCE in the presence of 200 μM CA in 0.05 M PB (pH 7) in Figure 8A. In

addition, the anodic peak currents for CA were verified for the several accumulation time started from 0 to 300 s, where the greater oxidation peak current was observed for 210 s. Thus, the modified electrode was adjusted with suitable accumulation time was considered to be 210 s for an effective oxidation of CA molecule. The reproducibility of the PSSS@f-MWCNTs/GCE modified electrode was achieved using five different modified GCE electrode in the presence of 200  $\mu\text{M}$  CA in 0.05 M PB (pH 7) with scanning rate ( $50 \text{ mV s}^{-1}$ ) was shown in Figure 8B. The PSSS@f-MWCNTs/GCE have great reproducible capability, and might be used for correct detection of CA. The storage stability of PSSS@f-MWCNTs/GCE were dignified by storing it at ambient temperature in air atmosphere for 4 weeks. The PSSS@f-MWCNTs/GCE was lost 2.8% of its original response after 4 weeks' storage.

### 3.8. Real time analysis

In order to calculate the applied capability of the PSSS@f-MWCNTs/GCE, for the determination of CA in wine. In this real time experiment, the two different marketable raw wine samples were used without any pretreated process. Then well-known concentration of CA was spiked, and their experimental recovery results were considered and tabulated in Table 2. It can be seen that PSSS@f-MWCNTs/GCE displays suitable recovery (97.6 to 98.3%) of CA in wine, which confirms the outstanding practicality of the PSSS@f-MWCNTs/GCE. The results also exposed that the PSSS@f-MWCNTs/GCE can be used for real time sensing of CA in potions.

**Table 2.** Determination of CA in wine samples using PSSS@f-MWCNT/GCE by DPV. (n = 3)

Samples	Added ( $\mu\text{M}$ )	Found ( $\mu\text{M}$ ) <sup>a</sup>	Recovery (%)	RSD (%) <sup>b</sup>
Wine sample 1	5	4.86	97.2	2.8
	10	9.23	92.3	2.3
	15	14.28	95.2	2.6
Wine sample 2	5	4.15	83	2.1
	10	9.86	98.6	2.4
	15	14.69	97.93	2.7

<sup>a</sup> Standard addition method. <sup>b</sup> Relative standard deviation for 3 measurements.

## 4. CONCLUSIONS

In this work, PSSS@f-MWCNTs nanocomposite was prepared, and characterized by XRD, FT-IR, SEM, TGA, DTA, and electrochemical methods. The electrochemical sensor performance was analyzed by CV and DPV towards CA. Voltammetric sensing application was established which revealed excellent analytical parameters such as LOD is 0.035  $\mu\text{M}$ , sensor range is 0.4–173.9  $\mu\text{M}$ , and sensitivity is 17.44  $\mu\text{A } \mu\text{M}^{-1}\text{cm}^{-2}$ . Also, the nanocomposite modified electrode has good selectivity and high stability, and excellent reproducibility.

## ACKNOWLEDGEMENTS

The National Science Council and The Ministry of Education, Taiwan supported this work. We would also like to acknowledge The Ministry of Science, and Technology, Taiwan (MOST 107-2113-M-027-005) for its financial support.

## References

1. S. Kogularasu, M. Govindasamy, S.-M. Chen, M. Akilarasan, and V. Mani, *Sensors and Actuators B: Chemical*, 253 (2017) 773-83.
2. M. Govindasamy, S.-M. Chen, V. Mani, M. Akilarasan, S. Kogularasu, and B. Subramani, *Microchimica Acta*, 184 (2017) 725-33.
3. M. Govindasamy, V. Mani, S.-M. Chen, T.-W. Chen, A.K. Sundramoorthy, *Scientific reports*, 7 (2017) 46471.
4. M. Govindasamy, S.-M. Chen, V. Mani, R. Devasenathipathy, R. Umamaheswari, K.J. Santharaj, et al., *Journal of colloid and interface science*, 485 (2017) 129-36.
5. R. Sasikumar, P. Ranganathan, S.-M. Chen, S.-P. Rwei, *Sensors and Actuators B: Chemical*, 255 (2018) 217-25.
6. S. Stankovich, D.A. Dikin, R.D. Piner, K.A. Kohlhaas, A. Kleinhammes, Y. Jia, et al., *carbon*, 45 (2007) 1558-65.
7. V. Mani, M. Govindasamy, S.-M. Chen, B. Subramani, A. Sathiyam, J.P. Merlin, *Int J Electrochem Sci*, 12 (2017) 258-67.
8. M. Govindasamy, V. Mani, S.-M. Chen, A. Sathiyam, J.P. Merlin, G. Boopathy, *Int J Electrochem Sci*, 11(2016) e10814.
9. A. Muthumariappan, M. Govindasamy, S.-M. Chen, K. Sakthivel, V. Mani, *Microchimica Acta*, 184 (2017) 3625-34.
10. V. Mani, T.-W. Chen, S. Selvaraj, *Int J Electrochem Sci*, 12 (2017) 7435-45.
11. Y. Zhu, S. Murali, W. Cai, X. Li, J.W. Suk, J.R. Potts, et al., *Advanced materials*, 22 (2010) 3906-24.
12. J.S. Bunch, S.S. Verbridge, J.S. Alden, A.M. Van Der Zande, J.M. Parpia, H.G. Craighead, et al., *Nano letters*, 8 (2008) 2458-62.
13. S. Manavalan, M. Govindasamy, S.-M. Chen, U. Rajaji, T.-W. Chen, M.A. Ali, et al., *Journal of the Taiwan Institute of Chemical Engineers*, 89 (2018) 215-223.
14. M. Akilarasan, S. Kogularasu, S.M. Chen, M. Govindasamy, T.W. Chen, M.A. Ali, et al., *Electroanalysis* 30 (2018) 1-10.
15. C. Gómez-Navarro, R.T. Weitz, A.M. Bittner, M. Scolari, A. Mews, M. Burghard, et al., *Nano letters*, 7 (2007) 3499-503.
16. F.-C. Chiang, C.-C. Chang, S.-M. Chen, T.-W. Chen, M. Govindasamy, H.-J. Yang, *Int J Electrochem Sci*, 13 (2018) 4613-24.
17. U. Rajaji, M. Govindasamy, S.-M. Chen, T.-W. Chen, X. Liu, S. Chinnapaiyan, *Composites Part B: Engineering*, 152 (2018) 220-30.
18. M. Govindasamy, S. Manavalan, S.-M. Chen, U. Rajaji, T.-W. Chen, F.M. Al-Hemaid, et al., *Journal of The Electrochemical Society*, 165 (2018) B370-B7.
19. L. Panchakarla, K. Subrahmanyam, S. Saha, A. Govindaraj, H. Krishnamurthy, U. Waghmare, et al., *Advanced Materials*, 21 (2009) 4726-30.
20. J.C. Meyer, A.K. Geim, M.I. Katsnelson, K.S. Novoselov, T.J. Booth, S. Roth, *Nature*, 446 (2007) 60.
21. J.S. Bunch, A.M. Van Der Zande, S.S. Verbridge, I.W. Frank, D.M. Tanenbaum, J.M. Parpia, et al., *Science*, 315 (2007) 490-3.
22. L. Chen, C. Yuan, H. Dou, B. Gao, S. Chen, X. Zhang, *Electrochimica Acta*, 54 (2009) 2335-41.
23. K. Nakanishi, N. Soga, *Journal of the American Ceramic Society*, 74 (1991) 2518-30.
24. J.H. Chen, C.-T. Ho, *Journal of agricultural and food chemistry*, 45 (1997) 2374-8.
25. A.S. Meyer, M. Heinonen, E.N. Frankel, *Food Chemistry*, 61 (1998) 71-5.

26. A. Ghiselli, M. Nardini, A. Baldi, C. Scaccini, *Journal of agricultural and food chemistry*, 46 (1998) 361-7.
27. V. Datsyuk, M. Kalyva, K. Papagelis, J. Parthenios, D. Tasis, A. Siokou, et al., *Carbon*, 46 (2008) 833-40.
28. J. Chen, F. Kobayashi, K. Eguchi, K. Waki, *Electrochemistry Communications*, 91 (2018) 25-30.
29. J. Guo, Q. Liu, C. Wang, M.R. Zachariah, *Advanced Functional Materials*, 22 (2012) 803-11.
30. Y. Shi, H. Xu, J. Wang, S. Li, Z. Xiong, B. Yan, et al., *Sensors and Actuators B: Chemical*, (2018) (in press)

© 2018 The Authors. Published by ESG ([www.electrochemsci.org](http://www.electrochemsci.org)). This article is an open access article distributed under the terms and conditions of the Creative Commons Attribution license (<http://creativecommons.org/licenses/by/4.0/>).